Journal of Applied Research in Water and Wastewater
E-ISSN: 2476-6283
Journal homepage: https://arww.razi.ac.ir

Mercury removal from industrial wastewater using activated carbon synthesized from natural shells

Rozita Moradi, Majid Mohadesi*

Department of Chemical Engineering, Faculty of Engineering, Kermanshah University of Technology, Kermanshah, Iran.

GRAPHICAL ABSTRACT

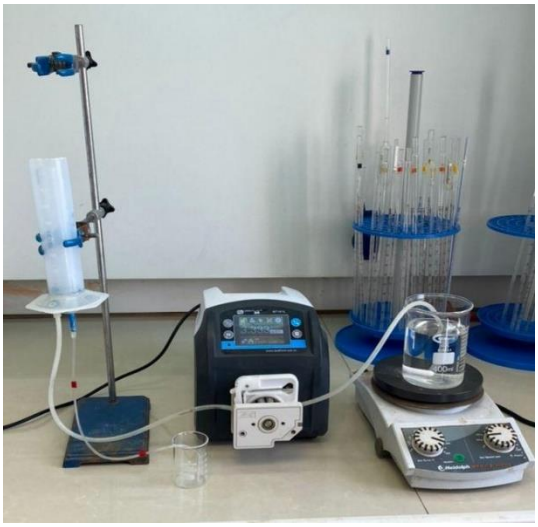

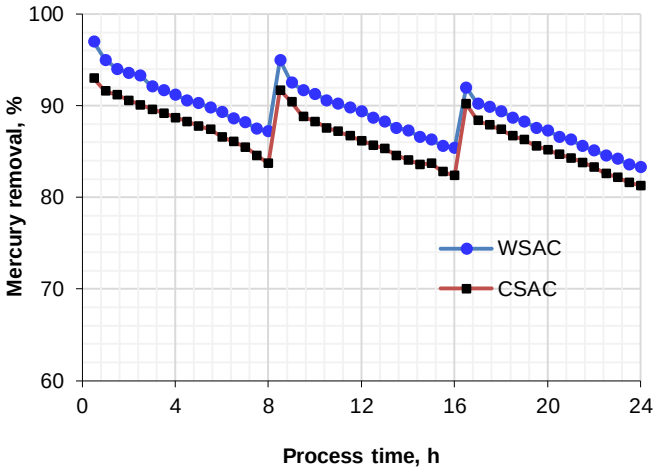

Reduction curve of coconut shells activated carbon and walnut shells activated carbon under optimal operating conditions

ARTICLE INFO

Article type:
Research Article

Article history:
Received 5 June 2025
Received in revised form 7 September 2025
Accepted 10 September 2025
Available online 30 December 2025

Keywords:
Activated carbon
Heavy metals
Natural shells
Mercury
Adsorption

ABSTRACT

The aim of this research was to separate mercury from gold refining wastewater using activated carbon (AC) from natural shells. To this end, walnut and coconut shells were used as the main source of AC. The characterizations of both ACs were compared by FTIR, BET, and SEM analyses. The FTIR results revealed interactions between the solute and the functional groups on the adsorbent surface. According to the BET results, the mean pore diameter (MPD) of AC from coconut shells (CSAC) was smaller than that derived from walnut shells (WSAC). The specific surface areas for CSAC and WSAC were 1069.1 and 119.6 m^2/g, respectively. SEM results revealed that the porous texture of ACs emanates from their cellular structure. This research further studied the impact of operational parameters “adsorbent dose” (0.3-3.8 g/L), “pH” (2-9), and “residence time” (10-120 min) on mercury removal. Under optimal operational conditions, the mercury removal rate reached 97% (for WSAC) and 93% (for CSAC). Kinetic model assessments revealed the highest agreement between the experimental data and the pseudo-first-order (PFO) model. Both adsorbents were regenerable, with their performance (compared to fresh adsorbents) exceeding 90% after each regeneration.

1. Introduction

The water crisis is a leading controversial challenge of the 21st century worldwide. Immense water scarcity and fast population growth have extremely threatened the lives of humans by contaminating water resources. Water pollution is due to industrial, chemical, agricultural, and toxic waste diffusion into water resources. Such contaminated water imperils human health, hygiene, and the environment, and imposes biological risks and issues to plants and animals. Heavy metals (HMs) are potent water pollutants due to their stability, toxicity, and bioaccumulation. Over the past decades, water pollution by HMs has been a subject of concern worldwide (Marichelvam and Azhagurajan, 2018). Population growth and recent scientific and technological breakthroughs have fostered agricultural and industrial activities, thereby intensifying the emergence and release of environmental pollutants. Pollutants are potent contributors to environmental disruption. Particularly, HMs are strongly in play due to their non-degradability and detrimental impacts on the health of living organisms and humans (Rajkumar *et al.*, 2010).

HMs infiltrate water and soil resources and their elevated water concentrations are deleterious to human health and water usability (Hou *et al.*, 2013). Furthermore, HMs hugely present in the soil are absorbed by plants, thereby interrupting plant metabolism and growth. Likewise, the immense soil concentrations of these metals are a serious

*Corresponding author Email: m.mohadesi@kut.ac.ir

Cite this article: R. Moradi, M. Mohadesi, Mercury removal from industrial wastewater using activated carbon synthesized from natural shells, *Journal of Applied Research in Water and Wastewater*, 12 (2), 2025, 136-143. doi: https://doi.org/10.22126/arww.2025.12281.1378

threat, as they can provoke soil structure destruction, yield reduction, declined biological activities, poor product quality, and diminished soil fertility. Besides, elevated levels of HMs in crops can harm human health by entering the food chains (Haydarpoor, SoltaniToolarood, and GoliKalanpa, 2017).

HMs are frequently present in industrial wastewater, the leading toxic pollutant concerning pollution intensity. HMs are hazardous and toxic even in trivial quantities. HMs are non-biodegradable and their environmental endurance is protracted. These elements accumulate in living tissues, and when their content exceeds an allowable threshold, they can inflict causes cancer, miscarriage, mutagenesis, and other unhealthy outcomes (Saleh, Sarı and Tuzen, 2017).

Toxic metals frequently found in water are arsenic (Ar), cadmium (Cd), chromium (Cr), lead (Pb), and mercury (Hg). The US Environmental Protection Agency defines these metals as precursor pollutants. Hg is a toxic metal characterized by its stability and bioaccumulation in the food chains. This metal has numerous industrial applications in painting, chloralkali process, pharmaceutical and electrical uses, fungicides, paper and pulp production, etc., and is a potent environmental pollutant. Hg, even in trivial quantities, is toxic to aquatic animals and plants. It affects humans by instigating conditions such as depression, chest pain, neurological disorders, pulmonary and renal function, nausea, vomiting, and shortness of breath *(Hadavifar et al.*, 2016; Liu *et al.*, 2018).

The most efficacious techniques for wastewater Hg removal are sulfide precipitation (Li, Liu and Deng, 2016), flocculation, coagulation (Bachand *et al.*, 2019), adsorption (Xia *et al.*, 2019; Ahmadi Kamarposhti, Bahramifar and Ehsani Tilami, 2022; Zarei *et al.*, 2022; Hossieni, Sohrabi and Akhlaghian, 2023; Hoveidamanesh *et al.*, 2025), ion exchange (Dabrowski *et al.*, 2004), electrodialysis, reduction, precipitation (Hua *et al.*, 2020), electrolysis, membrane filtration (Bandaru *et al.*, 2013), and biofiltration or a merge of these techniques (Li *et al.*, 2018; Zhang *et al.*, 2018). Of these, adsorption is a practical and affordable techniques for wastewater treatment from HMs. Indeed, adsorption is flexible in design and operation and can deliver huge volumes of purified wastewater. As adsorption is often reversible, adsorbents can be regenerated by a tailored regeneration processes. Activated carbon (AC) is the most potent adsorbent in removing HMs. This capacity emanates from a high volume of pores and micropores culminating in a high specific surface area (SSA) in AC (Fu and Wang, 2011).

Hg (Hg(II) and thimerosal) removal from pharmaceutical wastewater was studied utilizing F-400 granular AC at pilot and bench scales. Bench dynamic column experiments were carried out with the EBTC (empty bed times of contact) of 120, 90, 60, and 30 min. Under research conditions, the best Hg removal was attained using two GAC columns in series and a 30-min EBTC (total EBTC: 60 min) (Cyr, Suri and Helmig, 2002). Elsewhere, ACs were generated from organic sewage sludge employing chemical activation reagents "H_2SO_4", "H_3PO_4", and "$ZnCl_2$", followed by evaluating Hg(II) removal from aqueous solution by these ACs. Chemical activation markedly enhanced the quality of ACs. The maximum Hg(II) adsorption capacity was found in "$ZnCl_2$", followed by "H_3PO_4" and "H_2SO_4", all as ACs. Concerning Hg(II) concentration, solution pH, and the dosage of ACs, the results revealed a good agreement between the experimental data with the PFO equation and the Freundlich isotherm model (Zhang, Nriagu and Itoh, 2005).

Zhang, Yin and Liu (2017) studied Hg(II) and methylmercury adsorption on multi-walled carbon nanotubes (MWCNTs) modified with hydroxyl, amine, and carboxyl groups. They explored the impacts of diverse parameters (i.e., initial pH, natural organic matter, chlorine, and adsorbent dosage) on the adsorption efficiency. Amine-modified MWCNTs delivered substantial Hg(II) and methylmercury adsorption potency, with the pH-independent removal efficiency reaching 92% (Zhang, Yin and Liu, 2017). Sajjadi *et al.* (2018) produced pistachio wood waste-based AC (PWSAC) using ammonium nitrate as an activating agent. They characterized PWSAC and compared it with commercial ACs concerning morphological and textural properties, crystal structure, surface elemental composition, and surface chemistry. A pyrolysis temperature and time of 800 °C and 2 h, and a 5% saturation ratio were reported as optimal requirements for PWSAC preparation to realize maximum Hg(II) adsorption. Furthermore, the prepared PWSAC gained a SSA of 1448 m^2/g (Sajjadi *et al.*, 2018).

Budihardjo *et al.* (2021) studied AC production from coal and peat soil and used CaO (as a pH buffer) from oyster by-products to diminish Hg concentration in artificial landfill leachate. At variable pH levels, the equilibrium time for Hg reduction (by 81%) via adsorption was attained after 100 min. The adsorption capacity of AC on peat soil and coal was, respectively, 102 mg/g and 114 mg/g. They employed the Langmuir isotherm model as a tailored model for Hg adsorption. They concluded that peat soil/coal-based AC is an affordable adsorbent to treat landfill leachate (Budihardjo *et al.*, 2021). Ramírez-Rodríguez *et al.* (2023) compared the adsorption capacity of AC or polycaprolactone (PCL)-based whey protein fibrils (WPF) nanocomposites. At t: 30 °C and pH: 5, the maximum Hg adsorption was attained from AC (74.4 mg/g), AC/WPF (57.4 mg/g), and PCL/WPF (16.7 mg/g) nanocomposites. The adsorption capacity was raised at elevated temperatures, implying the endothermic nature of Hg adsorption using the research materials. They concluded that WPF is an affordably raw agent to remove Hg from polluted waters in industries and the environment (Ramírez-Rodríguez *et al.*, 2023). Elsewhere, based on hydrothermal carbonization (HTC) at 130 °C and for 4 h, Hugo *et al.* explored the properties of hydrocarbon generated from residual biomass of cocoa (*Theobroma cacao* L.). They reported 75.5% to 89.4% Hg removal rates, with adsorption capacities reaching 174.74 µg/g at a 30-minute residence duration (Hugo *et al.*, 2024).

Albatrni and Qiblawey (2024) proposed a novel technique to produce efficient environmentally-friendly AC for Hg removal from aqueous solutions. They used "sodium thiosulfate" and "walnut shells", respectively as "a renewable precursor" and "activating agent" for AC production. The produced AC had a total pore volume (TPV) of 0.303 cm^3/g and a SSA of 451.1 m^2/g. Under the research optimum conditions, the AC's maximum adsorption capacity reached 164.4 mg/g. Kinetically, the process was explained by the pseudo-second-order (PSO) and Freundlich isotherm models, implying the value of physical and chemical adsorption (Albatrni and Qiblawey, 2024). In another study, Albatrni *et al.* (2024) used potassium carbonate as a chemical activator to produce WSAC for Hg removal. The synthesized WSAC (as absorbent) had a TPV of 0.665 cm^3/g and a SSA of 1046.9 m^2/g. They further studied Hg removal efficiency under diverse factors, including pH, mass dose, temperature, initial Hg concentration, and residence time. At 35 ºC, the WSAC had a maximum adsorption capacity of 182.9 mg/g (Albatrni *et al.*, 2024).

When separating gold from wastewater, a leading challenge is the presence of HMs, possessing huge environmental risks. Nanosorbents hold a high surface-to-volume ratio and SSA, are non-toxic, and impose trivial environmental contamination. Hence, they are versatile candidates to remove HMs from wastewater. Taking note of these, the present research aims to separate Hg from gold purification wastewater using WSAC and CSAC (as adsorbents), concerning effective parameters of residence time, solution pH, and adsorbent dose.

2.1. 2. Experimental section

2.1. Materials

2.1.1. Adsorbents

WSAC and CSAC absorbents were used for Hg adsorption. Granular CSAC was obtained from Haycarb Company and granular WSAC was purchased from Elmisazan Pasargad Company (KANGAROO brand). Table 1 summarizes the specifications of both ACs.

Table 1. Characteristics of the adsorbents used in this research.

Parameter	CSAC	WSAC
Hardness, %	85	99
Density, kg/m^3	400	560
Ash, %	7	1.8
Humidity, %	5	2

2.1.2. Industrial wastewater

Industrial wastewater containing Hg complexes was obtained from the gold processing plant of Sari Guni Mine, Kurdistan, Iran. Table 2 presents the characteristics of the wastewater used in this research.

Table 2. Characteristics of the used wastewater in this study.

Property	Value
pH	10
COD, mg/L	400
BOD, mg/L	24
Hg concentration, mg/L	19

2.2. Experiments

All the experiments were performed in a continuous adsorption column. A certain volume of AC was placed in the adsorption column. Next, Hg-containing wastewater was added at a defined flow rate to the column using a pump. After the wastewater passed through the adsorption column, the samples were filtered using Whatman paper. Hg concentration in the final solution was determined with a DMA-80 evo device.

To determine the random error, all experiments were repeated three times, concerning the effects of residence time, solution pH, and adsorbent dose.

The adsorption capacity (q) and the percentage of Hg adsorbed (E) were obtained from Eqs. 1 and 2, respectively (Bansal and Goyal, 2005).

$$q = \frac{(C_0 - C_e)V}{W} \quad (1)$$

$$E = \frac{(C_0 - C_e)}{C_0} \times 100 \quad (2)$$

where, C_0 and C_e represent Hg's initial and final (equilibrium) concentrations (in mg/L), V represents the Hg-containing solution volume (in L), and W denotes the adsorbent's mass (in g). The equilibrium concentration is measured when the adsorption rate equals the desorption rate for the adsorbent and no noticeable changes in the concentration of mercury ions are observed over time.

2.3. Adsorption column

A cylinder (d: 1.5 cm, h: 19 cm) was selected as the adsorption column and its bottom was covered with a thin layer of glass wool. This layer was used to channel the flow and block the tube connected to the end of the adsorption column during the process. For each experiment, different amounts of adsorbent were loaded into the adsorption column. A Hg-containing wastewater solution with a certain concentration and a certain constant flow rate flowed continuously from the column's bottom. The flow rate of wastewater, which was connected to the end of the adsorption column by a tube from the tank, was controlled using a pump. Ultimately, the purified solution was discharged from the top of the adsorption column through a tube connected to the top of the column.

2.4. Effect of various parameters on Hg adsorption

The impacts of each variable were investigated by considering all other constant factors. Likewise, the residence time effect on Hg adsorption was investigated by two types of AC adsorbents, in time intervals of 10 to 120 min. In these conditions, 0.1 M hydrochloric acid was employed to adjust pH to 5. The dose of AC used was kept constant at 1.5 g/L. Since Hg precipitates at alkaline pHs, the studied pH was adjusted from 2 to 9 using sodium hydroxide and 0.1 M hydrochloric acid. After adjusting each of the desired pHs, a specific dose of AC (1.5 g/L) was added to the adsorption column and pH impacts on Hg adsorption was investigated by passing the Hg-containing wastewater solution and considering the optimal residence time.

Ultimately, the effect of AC dose (spanning from 0.3 to 3.8 g/L) on Hg adsorption from wastewater containing this HM was investigated, concerning that pH and residence time are considered at optimal values.

2.5. Adsorption kinetics

Kinetically, adsorption studies aim to measure the adsorption rate of adsorbents and the time it takes for the reactions to reach equilibrium. Regarding this, the most common method is to find the best adsorption kinetic equation. The Hg adsorption capacity per the adsorbent's unit weight for time t is calculated according to the Eq. 3:

$$q_t = \frac{(C_0 - C_t)V}{W} \quad (3)$$

where, C_t is the concentration (at t as time) of the Hg-containing solution (in g/L).

2.5.1. PFO model

The PFO model is based on the following assumptions (Wang and Guo, 2020). Adsorption occurs in regions where the adsorbed ions do not interact. Adsorption energy is independent of the absorbent's surface coverage. A saturated monolayer for the adsorbates on the adsorbent surface is associated with maximum adsorption. The adsorbate's concentration is assumed to be constant. For a metal ion, adsorption by AC follows a first-order rate equation. Upon integrating and applying the boundary conditions, the PFO model can be described as the following Eq.:

$$\ln(q_e - q_t) = \ln q_e - k_1 t \quad (4)$$

where, q_e and q_t denote the adsorbed capacity (in mg/g), respectively at "equilibrium" and "t as time". k_1 refers to the constant rate in the PFO model, and its value is obtained from the linear plot "$\ln(q_e - q_t)$" against "t".

2.5.2. PSO model

The assumptions considered for this model are consistent with the PFO model. Nonetheless, the adsorption of metal ions by AC in the PSO model is expressed by a second-order rate (SOR) equation. Considering the boundary conditions, the PSO model is ultimately given as the below Eq. (Wang and Guo, 2020).

$$\frac{t}{q_t} = \frac{1}{k_2 . q_e^2} + \frac{t}{q_e} \quad (5)$$

where, k_2 refers to the constant rate in the PSO model.

2.5.3. Weber-Morris Intraparticle Diffusion (WMID) model

Weber-Morris proposed the WMID model to identify the adsorption diffusion mechanism. This model explores whether the controlling step of the kinetic adsorption involves film diffusion, intraparticle diffusion, or both. The equation associated with this model is given below (Zhu, Moggridge and D'Agostino, 2016):

$$q_t = k_p . t^{0.5} \quad (6)$$

where, k_p denotes the intraparticle diffusion rate.

2.6. Reuse of adsorbents

First, the used AC was placed in an oven for 5 h (at 120 ºC) to remove its volatile compounds. Then, the obtained sample was placed inside the adsorption column of the laboratory setup, and deionized distilled water at 80 ºC was passed over the adsorbents by a pump for 4 h. After the regeneration process, the adsorbent was reused in the adsorption process.

2.7. Characterization of adsorbents

Fourier transform infrared (FTIR) analysis is a renowned spectroscopic technique in inorganic and organic chemistry and is used to determine the bonds in molecules and the type of functional groups. FTIR analysis was performed to assess adsorbents structurally. The adsorbents were examined by an AVATAR model FTIR device from Thermo at 400 to 4000 cm^{-1}.

The morphological and surface characteristics of the adsorbents used were studied by scanning electron microscopy (SEM) imaging. SEM is a sought-after microscopic technique that allows taking pictures by scanning the sample's superficial electron beams, thereby affording a high resolution of solid samples. To perform this test, an SEM device model MIRA III from TESCAN was used.

The BET test was employed to investigate and measure the SSA and determine the TPV and MPD of materials. Overall, porosity and SSA research is paramount in most applications. A BET device (model BELSORP MINI II, from BEL) was used to perform this test.

Direct mercury analyzer (DMA) is a popular device for analyzing liquid and solid samples. The process starts with a boat-based sample weighing, followed by sample exposure to thermal decomposition under an oxygen or air stream. Next, the remaining combustion product(s) and Hg flow into a catalyst. This step allows for the removal of interferences and, coincidently, Hg reduction and trap on a gold amalgamator, followed by releasing Hg into sorts of measuring cells placed along the spectrophotometer's optical path. As such, the signal-to-noise ratio is markedly mitigated by the dual beam of the DMA-80 evo, remarkably enhancing the limit of quantification and enabling accurate Hg determination reaching ppt levels. Such fostered signal stability enhances analysis reliability and reproducibility even at trivial quantities (Yang *et al.*, 2021). In this study, the DMA-80 evo device was used to determine Hg concentrations in primary and treated wastewater.

3. Results and discussion

3.1. Characterization of adsorbents

3.1.1. FTIR analysis

Fig. 1 presents FTIR spectra for CSAC before and after Hg adsorption. As demonstrated, the presence of three intense peaks at wavelengths of 3438, 1384, and 1112 cm^{-1}, as well as the vibration at wavelength 1633 cm^{-1} can be attributed, respectively, to "O-H stretching", "O-H bending", "C-O-C stretching", and "C=C stretching" vibrations (Hu *et al.*, 2018).

At wavelength 2922 cm^{-1} for this AC, the aldehyde family is observed in C-H stretching vibrations. By examining the bandwidth of the peaks present, it is evident that hydroxyl and carboxylic anhydride are the most important functional groups on the adsorbent surface (Hu *et al.*, 2018; Pettit, Irga and Torpy, 2018).

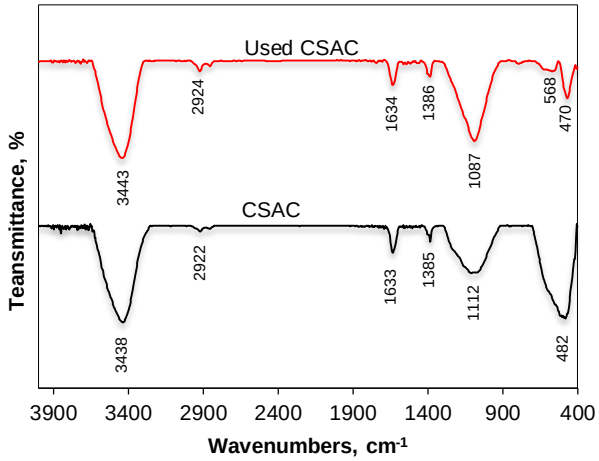

Fig. 1. FTIR spectrum for CSAC.

Fig. 2 depicts the results of FTIR spectroscopy for WSAC before and after Hg adsorption. At a wavelength of 2922 cm^{-1}, C-H stretching vibrational bonds from the aldehyde family are observed for this AC. In WSAC, the peaks at a wavelength of 3455 cm^{-1} are attributed to the vibrational hydroxyl (OH) groups, as well as to carboxyl (OH) bonds or phenolic (C-O) groups at a wavelength of 1126 cm^{-1}. Furthermore, the absorption bands identified in the wavelength range of 1380 to 1700 cm^{-1} represent carbonyl (C=O) and aromatic (CH) groups (Yu *et al.*, 2019; Li *et al.*, 2020). In the wavelength range of 2300-2400 cm^{-1}, there is a weak peak due to C=N bonds. The stretching vibrational bonds of C-H, H-O, and $CH=CH_2$ of the aromatic structure are located in the range of 500-800 cm^{-1} (Ghaedi *et al.*, 2015).

The strength and type of functional groups determine the adsorption capacity of ACs on their active sites. Ionic Hg reduction to metallic Hg has been observed as a spectroscopic result in many previous studies to interpret the mechanism of the Hg adsorption process (Johari et al., 2016; Ning *et al.*, 2018). After Hg adsorption, the change in peak intensity and their shift, particularly in the corresponding FTIR spectra, indicate the interactions of the adsorbent's superficial functional groups. Similar results are available in the literature on FTIR after Hg adsorption (Ning *et al.*, 2018; Li *et al.*, 2020).

The spectrum of CSAC at wavelength 3438 to 3442 cm^{-1} for OH stretching vibrational bond has shifted. Furthermore, wavelengths 1384 and 1112 cm^{-1} have shifted to wavelengths 1386 and 1087 cm^{-1}, respectively. For WSAC, a jump in peak intensity at wavelength 1574 cm^{-1} may be due to oxidation of the adsorbent's superficial hydroxyl groups and their conversion to carbonyl groups. From 500-800 cm^{-1}, the peaks related to C-H, H-O, and $CH=CH_2$ stretching vibrational bonds of the aromatic structure have further changed in peak intensity and shift. Hence, according to the above findings and the literature, the OH stretching vibrations associated with the hydroxyl group appear to play a decisive and important role in the adsorption process.

3.1.2. BET analysis

BET analysis results for both adsorbents are given in Table 3. These results indicate that CSAC has a smaller MPD, thereby holding a higher SSA, which both are in favor of the adsorption process. As shown, BET SSA is larger for CSAC compared to WSAC. The agreement of these data with previous research on these two ACs (Sebastián *et al.*, 2012, Zhang *et al.*, 2014) implies the acceptability of the obtained results.

Table 3. Results of BET analysis of surface characteristics of used adsorbents in this study.

Property	Unit	CSAC	WSAC
BET surface area	m^2/g	1069.1	119.6
Total pore volume	cm^3/g	0.467	0.069
Mean pore diameter	nm	1.747	2.298

3.1.3. SEM analysis

SEM images of the adsorbents used in this study are depicted in Fig. 3. This figure clearly reveals the porous texture of these raw materials, which emanates from the cellular structure. This porous structure enables the activating agent to infiltrate into raw materials. Parameters (e.g., TPV and MPD) are measured and evaluated in Table 3. As with Fig. 3, a lower dispersion in CSAC's pore size distribution can be observed compared to WSAC, which indicates a more homogeneous and uniform pore distribution of CSACs.

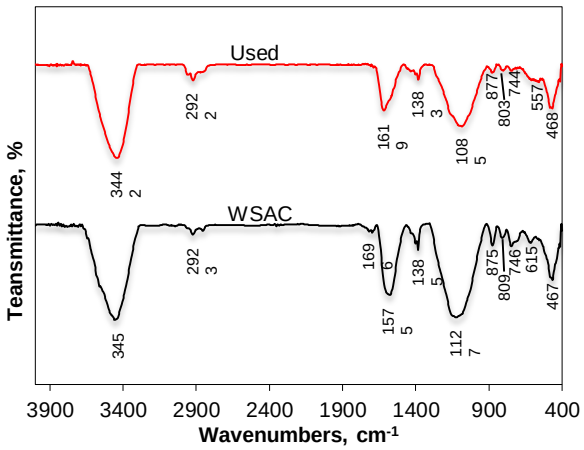

Fig. 2. FTIR spectrum for WSAC.

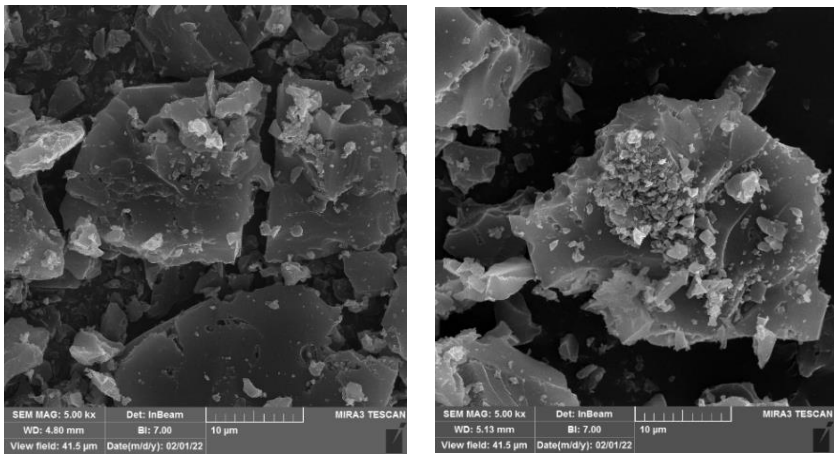

(a) **(b)**

Fig. 3. SEM images of adsorbent samples; (a) CSAC, (b) WSAC.

3.2.1. Residence time

Fig. 4 demonstrates the effects of residence time (i.e., 10 to 120 min) for both CSAC and WSAC. As shown, approximately 10% of the total Hg is adsorbed by the AC initially. After 45-60 min, the adsorption/removal rate by the processed AC is nearly constant and reaches equilibrium. After that, there is no marked change in the adsorption rate. Hence, a residence time of 45 min can be considered

the optimal residence time for the subsequent steps. Hg adsorption in the presence of WSAC is higher and its adsorption kinetics are faster in the first 10 min. Over time, despite continuous Hg adsorption, there is less tendency for Hg adsorption due to the adsorbent surface saturation, culminating in declined Hg removal efficiency.

3.2.2. pH

Fig. 5 depicts the impacts of solution pH (i.e., 2 to 9) on the removal rate of mercury by CSAC and WSAC. As shown, adsorption by WSAC is enhanced significantly at a pH greater than 3. The removal rate of Hg ions reaches a constant value at the pH of 5 and no comparable changes are observed at higher pHs. As with these results, a pH of 5 can be considered the optimal pH for both adsorbents.

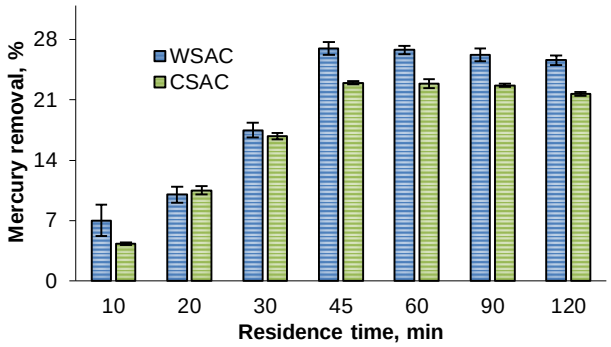

Fig. 4. Impacts of residence time on Hg removal from wastewater (pH: 5; adsorbent dose: 1.5 g/L).

A rise in the adsorption rate at pHs between 3 and 5 is probably due to the partial hydrolysis of the dominant species present in this pH range, which, with increasing pH and charging of the AC surface, has a greater tendency to adsorb on the adsorbent's superficial functional groups. Indeed, the formation of positively charged metal hydroxy groups in this pH range and their high tendency to adsorb surface functional groups both increase the adsorption rate of Hg. It appears that at low pHs, both the adsorbent and adsorbate have positive charges (H^+ and Hg^{2+}), which initiate the desorption reaction and reduce the adsorption rate.

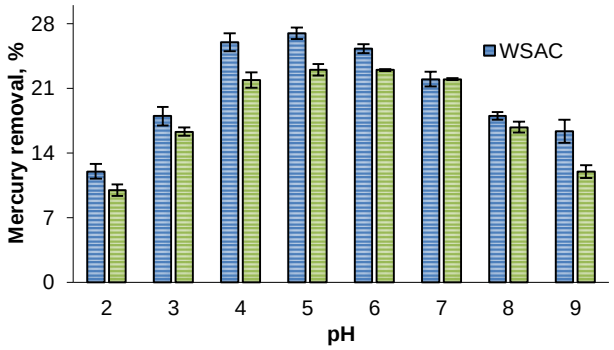

Fig. 5. Impacts of pH on Hg removal from wastewater (adsorbent dose: 1.5 g/L; residence time: 45 min).

3.2.3. Adsorbent dose

Regarding the optimal adsorbent dose required, Fig. 6 depicts the results of investigating the effect of adsorbent dose on the volume of Hg adsorption for CSAC and WSAC adsorbents. As shown, the adsorbent dose (a leading parameter in adsorption) naturally increases with increasing adsorbent dose.

Experiments in this research were carried out at adsorbent doses of 0.3 to 3.8 g/L at pH: 5 and residence time of 45 min (Fig. 6). As shown, with increasing adsorbent dose, the active and accessible sites for Hg ions increase and this improves the adsorption process. Next, this process continues until at a point the adsorption is nearly stabilized. As with the literature, this phenomenon is presumably due to the accumulation of adsorbent particles and the occurrence of an electrical repulsion force between adsorbent particles, which makes all adsorbent sites inaccessible to ions (Beless, Rifai and Rodrigues, 2014; Zhang *et al*., 2019). By increasing the WSAC dose (i.e., 1.5 to 3.0 g/L), the Hg ion removal efficiency increases from 27% to 94%. It is observed that the highest mercury removal efficiency is attained at a dose of 3.8 g/L for WSAC and CSAC, which were 97% and 93%, respectively.

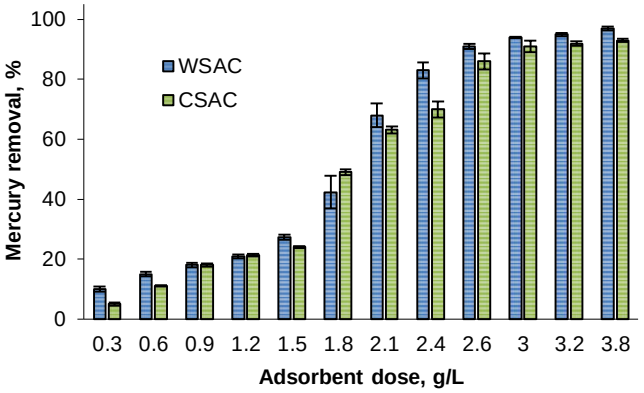

Fig. 6. Effect of adsorbent dose on Hg removal from wastewater (pH: 5; residence time: 45 min).

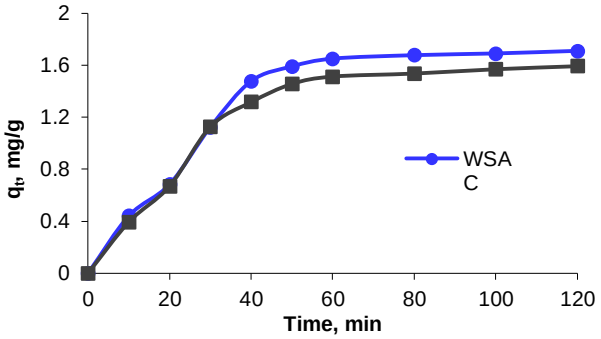

Fig. 7. Adsorption capacity of the adsorbents versus residence time under optimal operating conditions (pH: 5; adsorbent dose: 3.8 g/L).

3.3. Adsorption kinetics

Kinetic studies were conducted on laboratory data to assess the rate Hg adsorption rate by diverse adsorbents. The PFO, PSO, and WMID models were analyzed. Fig. 7 depicts the Hg adsorption capacity on CSAC and WSAC as a function of residence time. As depicted, WSAC reaches saturation or equilibrium adsorption capacity faster than CSAC.

To compare the kinetic properties of CSAC and WSAC adsorbents, Fig. 8 depicts the regression for each of the kinetic models. Likewise, Table 4 presents the constant parameters and coefficients of these models. As with Fig. 7 and Table 4, the R^2 value in the fit of experimental data and kinetic models when using both WSAC and CSAC adsorbents for the PFO model is closer to one. Also, comparing the calculated adsorption capacity using different kinetic models (PFO, PSO, and WMID) with the experimental adsorption capacity, shows that the relative error when using the PFO model is lower than the other two other models (PSO and WMID). So, the PFO model holds the maximum accuracy in predicting Hg adsorption capacity, followed by the PSO and WMID models. The PFO model advocates fast adsorption at initial times, as well as stabilized adsorption on the adsorbents over time.

3.4. Regeneration of adsorbents

As mentioned, the optimal conditions for Hg adsorption were obtained using both CSAC and WSAC adsorbents (pH: 5; adsorbent dose: 3.8 g/L; residence time: 45 min). Under these conditions, the adsorbents were used for a processing time of 24 h to reach about 90% of the initial efficiency (for WSAC, Hg adsorption is nearly 87%; for CSAC, Hg adsorption is nearly 84%). This time lasted for about 8 h for both adsorbents. After this time (about 8 h), the adsorbents were regenerated and reused. This process was repeated three times, with results revealing that adsorbents have a high ability to adsorb Hg after 24 h. Hence, when using WSAC and CSAC, adsorption efficiency is about 83% and 81%, respectively (Fig. 9). Based on the results, both adsorbents are renewable and have a performance higher than 90% compared to fresh adsorbents after each regeneration process. Furthermore, previous research implies that WSAC and CSAC are renewable for Hg adsorption (Larasati, Fowler and Graham, 2021; Lu *et al*., 2011; El Gamal *et al*., 2018).

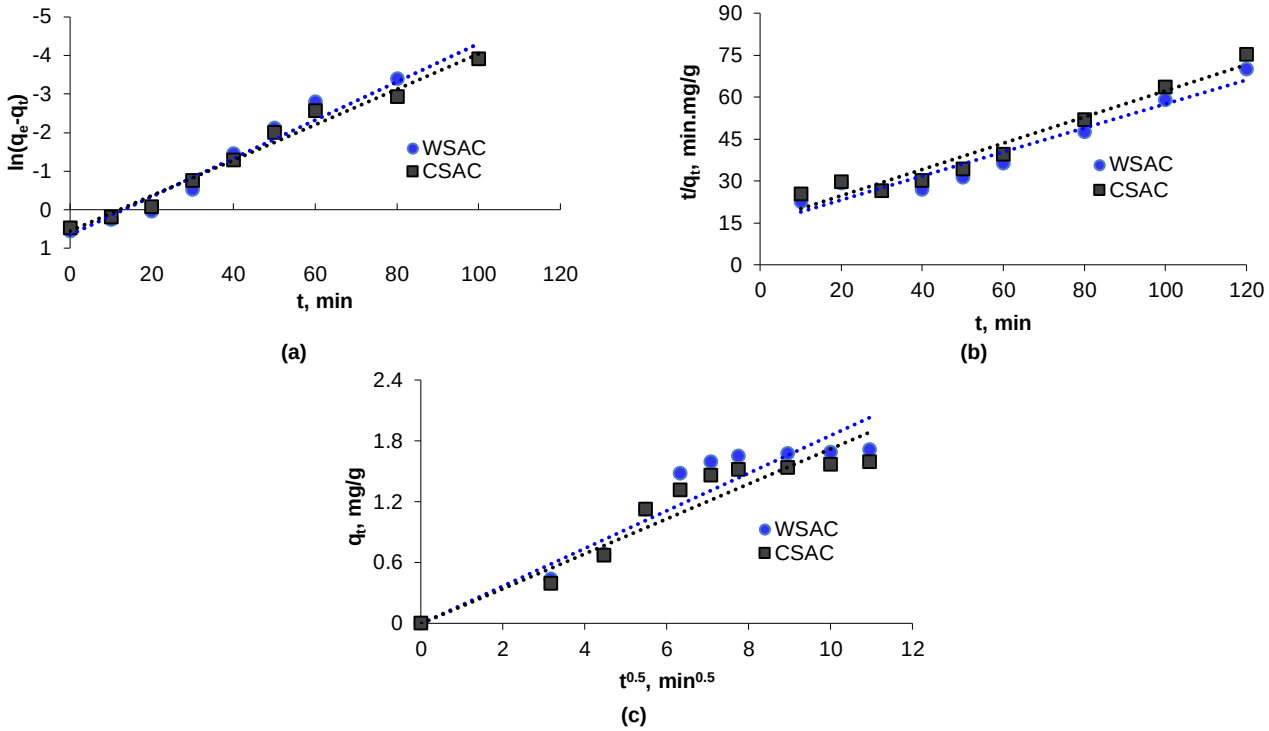

Fig. 8. Fitting of experimental data with kinetic models for Hg adsorption under optimal operating conditions (adsorbent dose: 3.8 g/L; pH: 5); a) PFO model, b) PSO model, c) WMID model.

Table 4. The parameters of kinetic models for Hg adsorption under optimal operating conditions (adsorbent dose of 3.8 g/L, pH of 5).

Adsorbent	CSAC	WSAC
$q_{e,exp}$, mg/g	1.59	1.71
Pseudo-first-order kinetic model		
q_e, mg/g	1.74	1.94
k_1, min^{-1}	0.0459	0.0497
R^2	0.9806	0.9659
Pseudo-second-order kinetic model		
q_e, mg/g	2.14	2.32
k_2, mg.g^{-1}.min^{-1}	0.0142	0.0127
R^2	0.9496	0.9391
Intraparticle diffusion model		
q_e, mg/g	2.03	1.88
k_p	0.1855	0.1719
R^2	0.8838	0.8905

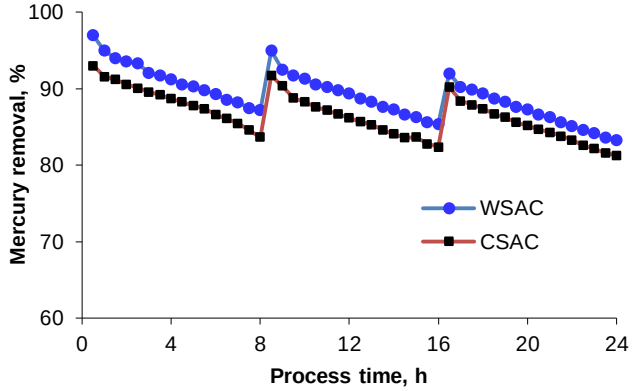

Fig. 9. Comparison of the reduction curve of CSAC and WSAC under optimal operating conditions (adsorbent dose: 3.8 g/L; pH: 5; residence time: 45 min).

4. Conclusions

This research assessed the presence of HMs in the wastewater resulting from gold separation as one of the problems of the gold industry, which poses great risks to the environment. The primary goal was to separate Hg from the wastewater resulting from gold purification using WSAC and CSAC. As such, the effective factors in Hg removal by AC adsorbents, including adsorbent dose (0.3-3.8 g/L), residence time (10-120 h), and pH (2-9), were investigated for the removal of Hg ions. WSAC outperformed CSAC in Hg adsorption. Adsorption kinetic models were employed to calculate the adsorption rate of both adsorbents and the time lasted for reactions to reach equilibrium. The PFO model better agreed with the experimental data, followed by the PSO and WMID models. Regarding regenerability, both WSAC and CSAC were regenerable and had a performance higher than 90% compared to the fresh adsorbent after each regeneration process.

Author contributions

Rozita Moradi: Data curation, Writing- Original draft preparation, Investigation
Majid Mohadesi: Supervision, Methodology, Software, Writing-Reviewing and Editing

Conflict of Interest

The authors declare no conflicts of interest.

Acknowledgment

The authors would like to sincerely thank Gold Processing Plant of Sari Guni Mine, Kurdistan, Iran, for making this research possible.

Data Availability Statement

All data, models, or code generated or used during the study are available in a repository or online.

References

Ahmadi Kamarposhti, E., Bahramifar, N., and Ehsani Tilami, S. (2022) 'Palm leaf ash as a biosorbent for improving the efficiency of the silver removal process,' *Journal of Applied Research in Water and Wastewater*, *9*(1), pp. 69-75. doi: https://doi.org/10.22126/arww.2021.5631.1183

Albatrni, H. *et al.* (2024) 'A green route to the synthesis of highly porous activated carbon from walnut shells for mercury removal,' *Journal of Water Process Engineering, 58*, p. 104802. doi: https://doi.org/10.1016/j.jwpe.2024.104802

Albatrni, H. and Qiblawey, H. (2024) 'Evaluation of sodium thiosulfate activated carbon for high-performance mercury removal from aqueous solutions,' *Environmental Technology & Innovation, 34*, p. 103621. doi: https://doi.org/10.1016/j.eti.2024.103621

Bachand, S. M. *et al.* (2019) 'Aluminum-and iron-based coagulation for in-situ removal of dissolved organic carbon, disinfection byproducts, mercury and other constituents from agricultural drain water,'

Ecological Engineering, 134, pp. 26-38. doi: https://doi.org/10.1016/j.ecoleng.2019.02.015

Bandaru, N. M. *et al.* (2013) 'Enhanced adsorption of mercury ions on thiol derivatized single wall carbon nanotubes,' *Journal of Hazardous Materials, 261*, pp. 534-541. doi: https://doi.org/10.1016/j.jhazmat.2013.07.076

Bansal, R. C. and Goyal, M. (2005) *Activated carbon adsorption*. 1st edn. Boca Raton: CRC press.

Beless, B., Rifai, H. S. and Rodrigues, D. F. (2014) 'Efficacy of carbonaceous materials for sorbing polychlorinated biphenyls from aqueous solution,' *Environmental Science & Technology, 48*(17), pp. 10372-10379. doi: https://doi.org/10.1021/es502647n

Budihardjo, M. A. *et al.* (2021) 'Mercury removal using modified activated carbon of peat soil and coal in simulated landfill leachate,' *Environmental Technology & Innovation, 24*, p. 102022. doi: https://doi.org/10.1016/j.eti.2021.102022

Cyr, P. J., Suri, R. P. and Helmig, E. D. (2002) 'A pilot scale evaluation of removal of mercury from pharmaceutical wastewater using granular activated carbon,' *Water Research, 36*(19), pp. 4725-4734. doi: https://doi.org/10.1016/S0043-1354(02)00214-2

Dabrowski, A. *et al.* (2004) 'Selective removal of the heavy metal ions from waters and industrial wastewaters by ion-exchange method,' *Chemosphere, 56*(2), pp. 91-106. doi: https://doi.org/10.1016/j.chemosphere.2004.03.006

El Gamal, M. *et al.* (2018) 'Bio-regeneration of activated carbon: A comprehensive review,' *Separation and Purification Technology, 197*, pp. 345-359. doi: https://doi.org/10.1016/j.seppur.2018.01.015

Fu, F. and Wang, Q. (2011) 'Removal of heavy metal ions from wastewaters: a review,' *Journal of Environmental Management, 92*(3), pp. 407-418. doi: https://doi.org/10.1016/j.jenvman.2010.11.011

Ghaedi, M. *et al.* (2015) 'Application of central composite design for simultaneous removal of methylene blue and Pb^{2+} ions by walnut wood activated carbon,' *Spectrochimica Acta Part A: Molecular and Biomolecular Spectroscopy, 135*, pp. 479-490. doi: https://doi.org/10.1016/j.saa.2014.06.138

Hadavifar, M. *et al.* (2016) 'Removal of mercury (II) and cadmium (II) ions from synthetic wastewater by a newly synthesized amino and thiolated multi-walled carbon nanotubes,' *Journal of the Taiwan Institute of Chemical Engineers, 67*, pp. 397-405. doi: https://doi.org/10.1016/j.jtice.2016.08.029

Haydarpoor, L., SoltaniToolarood, A., and GoliKalanpa, E. (2017) 'Evaluation of plant growth promoting traits of arsenic resistant bacteria and their effect on morphological properties of Origanum vulgare plant in an arsenic-polluted soil,' *Journal of Sol Biology, 4*(2), pp. 135-151. doi: http://dx.doi.org/10.22092/sbj.2017.109308

Hossieni, B., Sohrabi, S. and Akhlaghian, F. (2023) 'Processing date kernels for iron (III) and chromium (VI) adsorption from water,' *Journal of Applied Research in Water and Wastewater*, *10*(2), pp.179-187. doi: https://doi.org/10.22126/arww.2024.9132.1291

Hou, D. *et al.* (2013) 'Distribution characteristics and potential ecological risk assessment of heavy metals (Cu, Pb, Zn, Cd) in water and sediments from Lake Dalinouer, China,' *Ecotoxicology and Environmental Safety, 93*, pp. 135-144. doi: https://doi.org/10.1016/j.ecoenv.2013.03.012

Hoveidamanesh, F. *et al.* (2025) 'Removal of arsenic from ground water by modified Sabzevar zeolite,' *Journal of Applied Research in Water and Wastewater*, *12*(1), pp. 12-18. doi: https://doi.org/10.22126/arww.2025.8207.1268

Hu, S.-C. *et al.* (2018) 'Characterization and adsorption capacity of potassium permanganate used to modify activated carbon filter media for indoor formaldehyde removal,' *Environmental Science and Pollution Research, 25*, pp. 28525-28545. doi: https://doi.org/10.1007/s11356-018-2681-z

Hua, K. *et al.* (2020) 'Effective removal of mercury ions in aqueous solutions: A review,' *Current Nanoscience, 16*(3), pp. 363-375. doi: https://doi.org/10.2174/1573413715666190112110659

Hugo, R. O. *et al.* (2024) 'Production of hydrochar by low-temperature hydrothermal carbonization of residual biomass from cocoa production for mercury adsorption in acidic aqueous solutions,' *Case Studies in Chemical and Environmental Engineering, 10*, p. 100938. doi: https://doi.org/10.1016/j.cscee.2024.100938

Johari, K. *et al.* (2016) 'Adsorption enhancement of elemental mercury by various surface modified coconut husk as eco-friendly low-cost adsorbents,' *International Biodeterioration & Biodegradation, 109*, pp. 45-52. doi: https://doi.org/10.1016/j.ibiod.2016.01.004

Larasati, A., Fowler, G. D., and Graham, N. J. (2021) 'Insights into chemical regeneration of activated carbon for water treatment,' *Journal of Environmental Chemical Engineering, 9*(4), pp. 105555. https://doi.org/10.1016/j.jece.2021.105555

Li, Q., Liu, T., and Deng, P. (2016) 'Recovery of mercury and lead from wastewater by sulfide precipitation-flotation,' *Characterization of* Minerals*, Metals, and Materials, 2015*, pp. 667-674. doi: https://doi.org/10.1007/978-3-319-48191-3_84

Li, Y. *et al.* (2018) 'Alkynyl carbon materials as novel and efficient sorbents for the adsorption of mercury (II) from wastewater,' *Journal of Environmental Sciences, 68*, pp. 169-176. doi: https://doi.org/10.1016/j.jes.2016.12.016

Li, Z., *et al.* (2020) 'Adsorption of congo red and methylene blue dyes on an ashitaba waste and a walnut shell-based activated carbon from aqueous solutions: Experiments, characterization and physical interpretations,' *Chemical Engineering Journal, 388*, pp. 124263. doi: https://doi.org/10.1016/j.cej.2020.124263

Liu, C. *et al.* (2018) 'Mercury adsorption from aqueous solution by regenerated activated carbon produced from depleted mercury-containing catalyst by microwave-assisted decontamination,' *Journal of Cleaner Production, 196*, pp. 109-121. doi: https://doi.org/10.1016/j.jclepro.2018.06.027

Lu, P.-J. *et al.* (2011) 'Chemical regeneration of activated carbon used for dye adsorption,' *Journal of the Taiwan Institute of Chemical Engineers, 42*(2), pp. 305-311. doi: https://doi.org/10.1016/j.jtice.2010.06.001

Marichelvam, M., and Azhagurajan, A. (2018) 'Removal of mercury from effluent solution by using banana corm and neem leaves activated charcoal,' *Environmental Nanotechnology, Monitoring & Management, 10*, pp. 360-365. doi: https://doi.org/10.1016/j.enmm.2018.08.005

Ning, P. *et al.* (2018) 'Adsorption-oxidation of hydrogen sulfide on Fe/walnut-shell activated carbon surface modified by NH_3-plasma,' *Journal of Environmental Sciences, 64*, pp. 216-226. https://doi.org/10.1016/j.jes.2017.06.017

Pettit, T., Irga, P., and Torpy, F. (2018) 'Functional green wall development for increasing air pollutant phytoremediation: Substrate development with coconut coir and activated carbon,' *Journal of Hazardous Materials, 360*, pp. 594-603. doi: https://doi.org/10.1016/j.jhazmat.2018.08.048

Rajkumar, M. *et al.* (2010) 'Potential of siderophore-producing bacteria for improving heavy metal phytoextraction,' *Trends in Biotechnology, 28*(3), pp. 142-149. doi: https://doi.org/10.1016/j.tibtech.2009.12.002

Ramírez-Rodríguez, L. C. *et al.* (2023) 'Comparison of adsorption performance of nanocomposite materials of whey protein nanofibrils, polycaprolactone and activated carbon for mercury removal,' *Environmental Nanotechnology, Monitoring & Management, 20*, pp. 100826. doi: https://doi.org/10.1016/j.enmm.2023.100826

Sajjadi, S.-A. *et al.* (2018) 'Efficient mercury removal from wastewater by pistachio wood wastes-derived activated carbon prepared by chemical activation using a novel activating agent,' *Journal of Environmental Management, 223*, pp. 1001-1009. doi: https://doi.org/10.1016/j.jenvman.2018.06.077

Saleh, T. A., Sarı, A., and Tuzen, M. (2017) 'Optimization of parameters with experimental design for the adsorption of mercury using polyethylenimine modified-activated carbon,' *Journal of Environmental Chemical Engineering, 5*(1), pp. 1079-1088. doi: https://doi.org/10.1016/j.jece.2017.01.032

Sebastián, D. *et al.* (2012) 'Enhanced oxygen reduction activity and durability of Pt catalysts supported on carbon nanofibers,' *Applied Catalysis B: Environmental, 115*, pp. 269-275. https://doi.org/10.1016/j.apcatb.2011.12.041

Wang, J., and Guo, X. (2020) 'Adsorption kinetic models: Physical meanings, applications, and solving methods,' *Journal of Hazardous Materials, 390*, pp. 122156. doi: https://doi.org/10.1016/j.jhazmat.2020.122156

Xia, M. *et al.* (2019) 'Removal of Hg (II) in aqueous solutions through physical and chemical adsorption principles,' *RSC Advances, 9*(36), pp. 20941-20953. doi: https://doi.org/10.1039/c9ra01924c

Yang, Y. *et al.* (2021) 'Reaction mechanism of elemental mercury oxidation to Hg_SO_4 during SO_2/SO_3 conversion over V_2O_5/TiO_2 catalyst,' *Proceedings of the Combustion Institute, 38*(3), pp. 4317-4325. doi: https://doi.org/10.1016/j.proci.2020.10.007

Yu, Q. *et al.* (2019) 'Characterization of metal oxide-modified walnut-shell activated carbon and its application for phosphine adsorption: equilibrium, regeneration, and mechanism studies,' *Journal Wuhan University of Technology, Materials Science Edition, 34*, pp. 487-495. doi: https://doi.org/10.1007/s11595-019-2078-y

Zarei, M. *et al.* (2022) 'Removal of lead and cadmium with an optimized composite of expanded graphite/g-C_3N_4/phenylenediamine,' *Journal of Applied Research in Water and Wastewater*, *9*(2), pp. 154-166. doi: https://doi.org/10.22126/arww.2023.8253.1269

Zhang, B. *et al.* (2014) 'Synthesizing nitrogen-doped activated carbon and probing its active sites for oxygen reduction reaction in microbial fuel cells,' *ACS Applied Materials & Interfaces, 6*(10), pp. 7464-7470. doi: https://doi.org/10.1021/am5008547

Zhang, C. *et al.* (2019) 'Adsorption behavior of engineered carbons and carbon nanomaterials for metal endocrine disruptors: experiments and theoretical calculation,' *Chemosphere, 222*, pp. 184-194. doi: https://doi.org/10.1016/j.chemosphere.2019.01.128

Zhang, D., Yin, Y. and Liu, J. (2017) 'Removal of Hg2+ and methylmercury in waters by functionalized multi-walled carbon nanotubes: adsorption behavior and the impacts of some environmentally relevant factors,' *Chemical Speciation & Bioavailability, 29*(1), pp. 161-169. doi: https://doi.org/10.1080/09542299.2017.1378596

Zhang, F.-S., Nriagu, J. O. and Itoh, H. (2005) 'Mercury removal from water using activated carbons derived from organic sewage sludge,' *Water Research, 39*(2-3), pp. 389-395. doi: https://doi.org/10.1016/j.watres.2004.09.027

Zhang, Q. *et al.* (2018) 'A facile method to prepare dual-functional membrane for efficient oil removal and in situ reversible mercury ions adsorption from wastewater,' *Applied Surface Science, 434*, pp. 57-62. doi: https://doi.org/10.1016/j.apsusc.2017.09.230

Zhu, Q., Moggridge, G. D. and D'Agostino, C. (2016) 'Adsorption of pyridine from aqueous solutions by polymeric adsorbents MN 200 and MN 500. Part 2: Kinetics and diffusion analysis,' *Chemical Engineering Journal, 306*, pp. 1223-1233. doi: https://doi.org/10.1016/j.cej.2016.07.087